Int Ophthalmol (2019) 39:1939–1947
https://doi.org/10.1007/s10792-018-1023-y

ORIGINAL PAPER

# Three-dimensional surface presentation of optic nerve head from SPECTRALIS OCT images: observing glaucoma patients

**Abdel-Razzak M. Al-hinnawi · Arqam M. Alqasem · Bassam O. Al-Naami**

Received: 19 June 2018 / Accepted: 14 September 2018 / Published online: 24 September 2018


**Abstract**
*Purpose* To propose an innovative three-dimensional *surface* presentation of the optic nerve head (ONH) from the SPECTRALIS optical coherence tomography (OCT) device.
*Method* A dataset of OCT ONH files from eight glaucoma follow-up patients was obtained. The set consisted of OCT ONH images for 20 right eyes (OD) and 17 left eyes (OS). Preprocessing steps followed with OCT reconstruction procedures were designed. The three-dimensional (3D) surface rendering was generated for all OCT ONH images. A set of eight International Organization for Standardization (ISO) roughness parameters were calculated to assess the disparities in the 3D ONH surface morphology during follow-up visit.
*Results* The 3D ONH surface presents a new OCT display to ophthalmology; so, the physician can examine the *surface morphology* of the OCT ONH region. The 3D ONH surface's shape varied noticeably during follow-up visits in glaucoma patients. The percentage disparity of ONH surface roughness's can be as small as 3% or almost zero, but it can be as large as 56% or 100%.
*Conclusions* The approximation of OCT ONH 3D surface is feasible; it may possibly be beneficial to ophthalmology. It allows ophthalmologist to perceive the *entire* changes in the ONH surface morphology during the follow-up attendances; so, it can be used to observe patient health. The ISO roughness measurements are suggestive complementary factors to observe the alterations in the OCT ONH region.

**Keywords** Optical coherence tomography · Optic nerve head · 3D surface visualization · Glaucoma

**Electronic supplementary material** The online version of this article (https://doi.org/10.1007/s10792-018-1023-y) contains supplementary material, which is available to authorized users.

A.-R. M. Al-hinnawi (✉)
Faculty of Allied Health Sciences, Medical Imaging Department, The Hashemite University, P.O. Box 330127, Zarqa 13133, Jordan
e-mail: hinawiabed@hu.edu.jo

A. M. Alqasem
ISHRAQ Eye Centre, Amman 11183, Jordan
e-mail: Arqam_al_qasem@hotmail.com

B. O. Al-Naami
Faculty of Biomedical Engineering, The Hashemite University, P.O. Box 330127, Zarqa 13133, Jordan
e-mail: b.naami@hu.edu.jo

## Introduction

Optical coherence tomography (OCT) employs coherence optical gating in order to obtain two-dimensional (2D) cross section of the retina and optic nerve [1–4]; hence, in the ophthalmology clinic, it permits observing any defects in the thickness of the retinal nerve

fiber layer (RNFL) and any variations in the shape of the optic nerve head (ONH) [4]. The RNFL and ONH are subject to be affected due to eye diseases such as glaucoma [4–7]. The thickness of RNFL remains the prevailing factor for observing the variations of the intraocular pressure in the eye [5, 6]. However, several 2D parameters have been utilized to observe variations in the morphology of ONH (e.g., axial length, cup-to-disc ratio, ganglion cell complex, optic disc area and optic disc rim area, the nasal and temporal ONH incline measures) [7–9]. Volumetric parameters (e.g., ONH's cup volumes) have also been calculated based on landmarks that were set by the ophthalmologist [8, 10].

On the other hand, due to the advances in computer sciences, the three-dimensional (3D) visualization of data from diagnostic medical imaging has reached medicine; the 3D medical imaging visualization can disclose occult information to reach the precise medical decision about patient's health [11]. Therefore, some researchers explored the 3D visualization techniques on OCT images [12–16]. They evaluated the benefit of 3D volume rendering of different human eye's structures appeared in OCT images.

This paper introduced new presentations of the *surface rendering* of the ONH from SPECTRALIS OCT examinations. The OCT coronal slices of the ONH region were displayed. The 3D surface of the ONH region was visualized. Both presentations, to the best of our knowledge, have not been reported in OCT. The suggested technique demonstrated the entire 3D shape of ONH valley from top to bottom (i.e., the lamina cribrosa). We observed this new 3D ONH surface presentation on a set of glaucoma follow-up patients. The variations in the 3D ONH surface's shape were assessed by means of ISO roughness parameters, which, to best of our knowledge, have not been investigated. The results showed that the 3D ONH surface could prevail complementary information that may possibly benefit ophthalmology sciences. Since the experiments were done on 3D volumes of OCT images, supplementary videos for illustrations were attached with this paper. The paper presents technical findings, medical validation is a prospective research.

## Materials

OCT files were obtained for eight patients who had multiple visits to a private ophthalmology clinic (*ISHRAQ* eye center) in Amman, Jordan, in the past 2 years (2016–2017). All patients were from Jordan (5 males, 3 females, range of ages: 12–77 years). Six patients had two follow-up visits, but the OCT files for left eye were missing for one of those patients, one patient (age 12) had three follow-up visits, and one patient (age 13) had five follow-up visits for right eye and four follow-up visits to left eye. In each visit, the patient enrolled OCT examinations using a 2D spectral domain OCT device (SPECTRALIS® Laser Tracking Tomography made by Heidelberg Engineering in Germany). Hence, in total, the dataset consisted of 37 OCT ONH exams (20 right and 17 left eyes). All eyes suffered from variable severity of glaucoma according to Heidelberg Eye Explorer (software) version 6.9.5. For each eye, the OCT file of the ONH region was used. The supplementary file, called as "original OCT ONH video," illustrates one of the original OCT files. Each OCT file contained two presentations of the ONH region as shown in Fig. 1 (Still Frame). On the left side, there is a video showing the location of 24 slices that are confined in a green circle including the whole ONH region and its surroundings (circle diameter is 3.5 mm), while, on the right side, there is an animation of the 24 2D cross sections of ONH and part of the retina. The latter is usually called as the "B-Scan mode" of the ONH. The two displays are concatenated to form a single $1262 \times 496$ matrix. The spatial resolution was set to 2 μm, and they were displayed as RGB colored image. All files were saved and later processed in a personnel computer (PC) with the following main specifications: Intel ® Core™ i7-4790 CPU@3.6 GHz, 64 bits, and 8.00 GB RAM. The PC was equipped with "ImageJ" program (i.e., Image Processing and Analysis in JAVA) and "Surfer 3D Viewer" program. Both platforms were used to accomplish the experiments.

## Methods

The experiments were performed on the ONH B-scan mode. Each 2D cross section image in the B-scan shows the variations in the *morphology* (i.e., the valley shape) of the ONH within a slice of one of the 24 slices

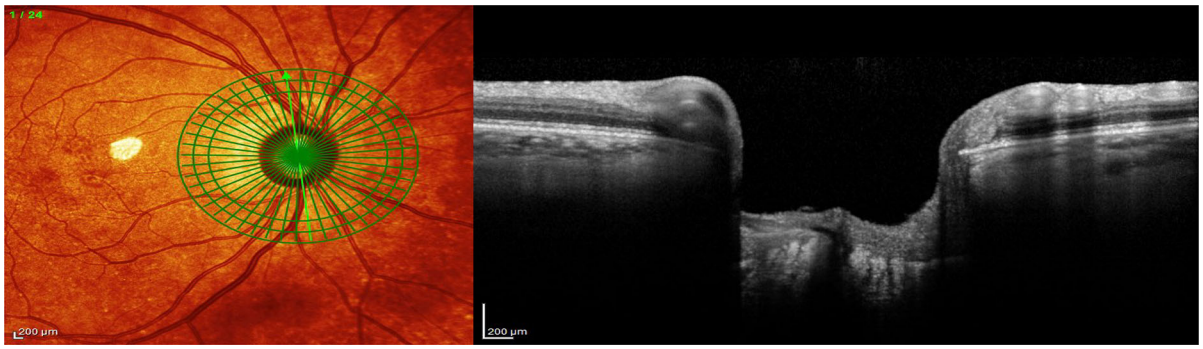


**Fig. 1** The first frame out of 24 frames for one of the OCT ONH right eye

(Fig. 1. right). Figure 2 shows the block diagram of the method that was developed to generate the 3D surface of the ONH. All experiments were performed in accordance with research ethics and guidelines. The research did not contain any studies with human participants (volunteers) performed by any of the authors. The OCT cases, used in the experiments, are old examinations. The patient's identifications were removed from all OCT files, so they become as anonymous OCT images. For this type of study, formal consent is not required in our institution. The study was approved by the Research Committee ISHRAQ Eye Centre in Amman, Jordan.

The method consisted of five steps. First, we extracted the 710 × 496 × 24 video from the B-scan of the OCT file. This resulted in a 3D volume consisting of 710 × 496 of 24 cross sections in the ONH and its surroundings. Each cross section in the video included the optic nerve cup, neuro-retinal rim, and part of the RNFL. The video was converted from RGB to 16 bits grayscale to speed-up the post-processing steps. Second, a 3D median filter in a 5 × 5 × 5 window was applied. This yielded to smooth the RNFL and ONH as well as it remarkably removed the small OCT mottles occurring in the vitreous chamber of the eye, as shown in the second supplementary file called as "the Smoothed B-Scan of the OCT ONH region." Third, the B-scan video was re-sliced (reconstructed) from top to bottom retaining the original image resolution (i.e., without interpolation). This resulted in a 710 × 24 × 496 video. Since there was only 24 slices in the original B-scan, the width of each image in the resulting video was small (only 24 rows). Therefore, the video y-axis (width)

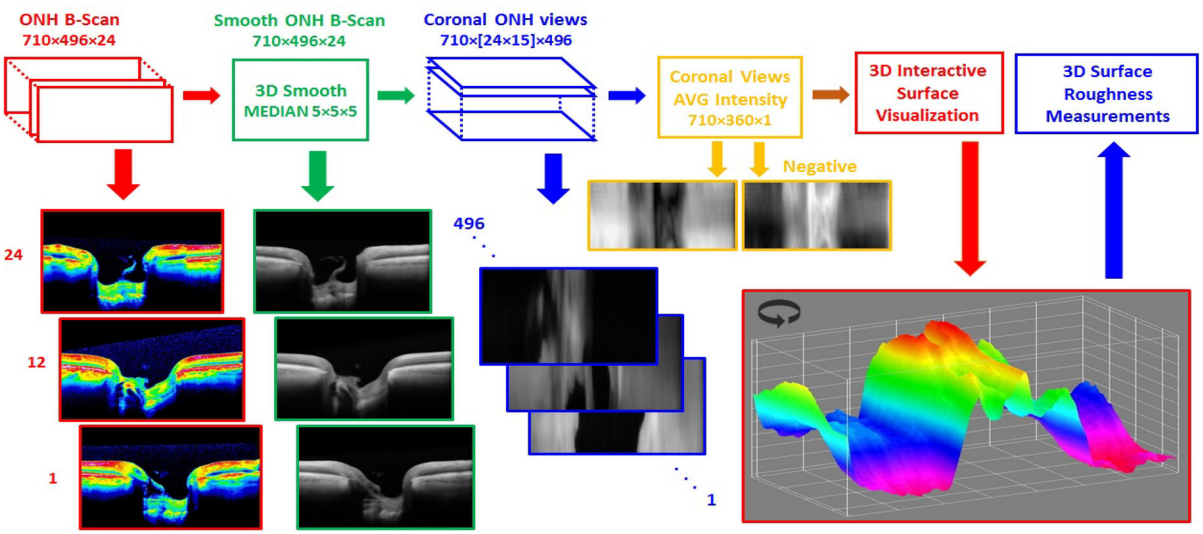


**Fig. 2** The block diagrams for OCT 3D ONH cup surface

was scaled by a factor equal to 15. This yielded to 710 × 360 × 496 video. The value equal to 15 was chosen because this led to width of 360 pixels, which would have been the expected width if the SPECTRALIS device had generated the whole available 360 slices of the green circle encompassing the ONH region instead of 24 (the first supplementary file). This video was called as the *coronal* slices of the OCT ONH. It shows the serial ONH coronal shape variations starting at the ONH edges and continually narrowing toward the deepest point of the optic nerve (toward the Lamina Cribrosa). The third supplementary file, named as "The coronal slices of OCT ONH region," shows a demonstration.

In the fourth step, the average intensity of the 496 coronal slices of the ONH region was calculated. This resulted in a single image of size of 710 × 360 × 1 pixels as seen in Fig. 3 (left). Thus, the retina areas appear bright shades, while the ONH cup's regions appear dark in Fig. 3 (left). For the sake of further illustration, Fig. 3 (middle) shows the negative image, while Fig. 3 (right) shows the RGB colored image of the negative image. It is important to note that these images (Fig. 3) present OCT information in different manner from the original OCT file (Fig. 1). Finally, in the fifth step, 3D *surface rendering* was utilized to display the averaged coronal ONH region in Fig. 3 (right). The 3D surface visualization revealed the variations in the 3D morphology of the ONH surface (Fig. 4). It was developed so the user (ophthalmologist) could rotate the ONH 3D view to observe any differences during the successive visits of the patient. The "Red–Green–Blue (RGB) look-up-table LUT" color plate was utilized. This color plate employs the RGB rainbow color order, so the red represents the highest intensity value while the violet represents the lowest. Therefore, using the image in Fig. 3 (middle), the deep points of the ONH were presented by green-to-red spectrum colors, while the ONH edges and the retina parts were presented by blue-to-violet colors.

The 3D surface's morphology can be described by calculating roughness parameters; they are also called as waviness parameters. Therefore, we measured roughness of the ONH surface in Fig. 3. There are international roughness parameters such as those described in ISO 25178-2 and ISO 4287-2000 standards (Ref. No. 17 and 18). A set of seven common parameters were selected. They are the arithmetic mean deviation ($R_a$), the root-mean-square deviation ($R_q$), the kurtosis of the deviation ($R_{ku}$), the skewness of the deviation ($R_{sk}$), the lowest surface valley ($R_v$), the highest surface peak ($R_p$), and the total surface height ($R_t$) of the ONH surface. These parameters can be calculated in ImageJ with correspondence to ISO 4287-2000. They are all based on the amplitude (intensity) of each pixel in Fig. 3. Also, the sum of the pixel intensities was measured; it was denoted as roughness integrated density ($R_{IntDen}$). It was normalized by dividing its value by the size of the image (710 × 360). Hence, eight roughness parameters were assessed. Our objective was to quantify and monitor the variations in the ONH surface after the successive visits to ophthalmology clinic.

## Results

The 3D ONH surface was generated of each eye (right and left) for all patients in each follow-up visit. This was done using the "Surfer 3D viewer" program. Figure 4 illustrates the 3D ONH surface displays for three different patients who had two, three, and five

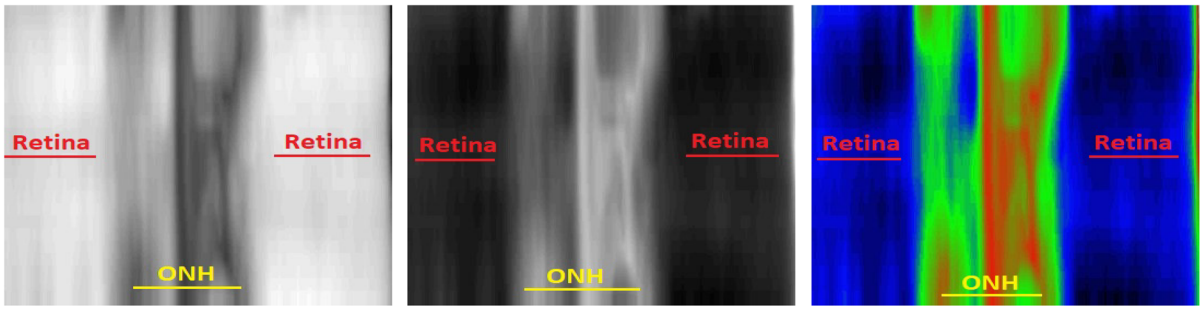


**Fig. 3** The average image of the 496 coronal slices of the ONH cup of right eye (left). The RGB colored image (right) of the negative image (middle)

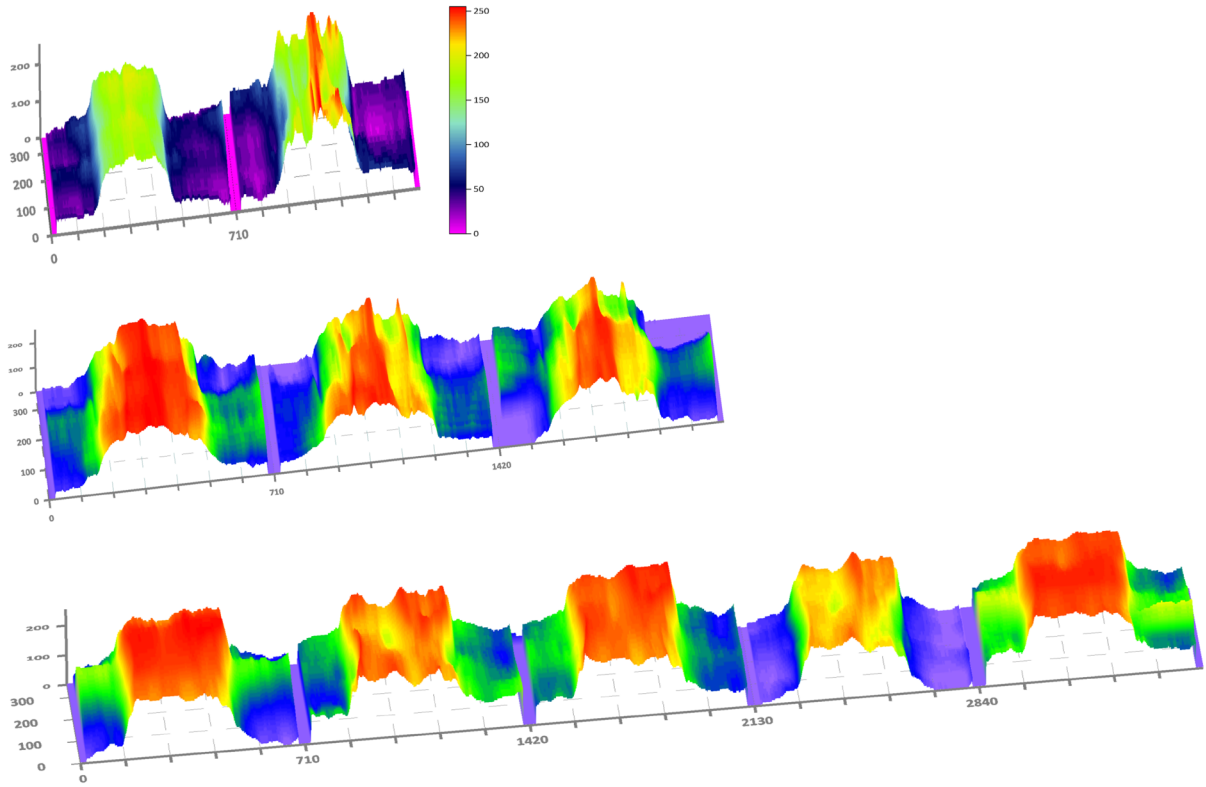


**Fig. 4** The 3D surface of OCT ONH region during two (**a**), three (**b**), and five (**c**) follow-up visits

follow-up visits. This figure demonstrates that there are *perceivable* (visible) differences in the shape of the ONH surface. This finding was repeated for all eyes in the dataset. In other words, there was disparity in the shape of the 3D surface of the ONH region for all glaucoma patients in their follow-up visits. Each 3D visualization in Fig. 4 was designed to permit the ophthalmologist to observe the ONH appearance from different angels in accordance to rotation parameters for x-, y-, and z-axis in the 3D view. The supplementary video named as "3D OCT ONH surface with rotation" illustrates an example of 3D OCT ONH surface rotating around z-axis located at the center of ONH valley.

In order to quantify the ONH surface variations, the selected eight roughness parameters ($R_a$, $R_q$, $R_{ku}$, $R_{sk}$, $R_v$, $R_p$, $R_t$, and $R_{IntDen}$) were calculated. This was done for all eyes in the dataset. For example, Fig. 5 shows the average roughness ($R_a$) measurements on all right and left eyes for all patients. It shows that $R_a$ decreases or increases during the successive visits to ophthalmology clinic. Thus, we measured the disparities in the value of each one of these eight roughness parameters during all follow-up visits. Then, we calculated the average (AVG), standards deviation (STDEV), maximum value (MAX), and minimum value (MIN) of the disparities for all follow-up patients. Figures 6 and 7 show bars indicating the limit values of summing ''AVG ± half STDEV'' of roughness disparities for right and left eyes, respectively. Each bar is crossed by a line showing the MAX and MIN disparity for each roughness parameter. The x-axis shows the numerical results labeled in tables. Both figures proved, quantitatively, that there were inequalities of ONH region's waviness during follow-up visits, as visually noted in Fig. 4.

## Discussion and conclusions

From technical point of view, this paper continued previous investigation on the geometry of ONH from SPECTRALIS OCT images [9]. However, instead of the ONH incline-slope quantities that previously

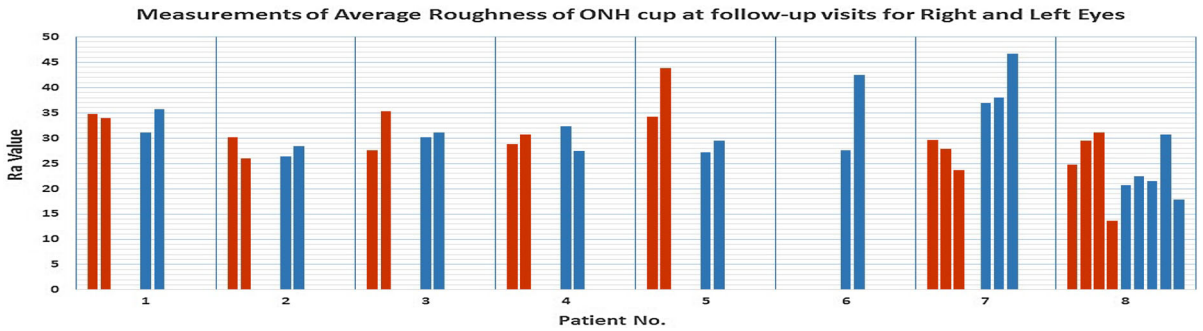


**Fig. 5** A chart showing the average roughness ($R_a$) measurements on all right (blue bars) and left eyes (red bars)

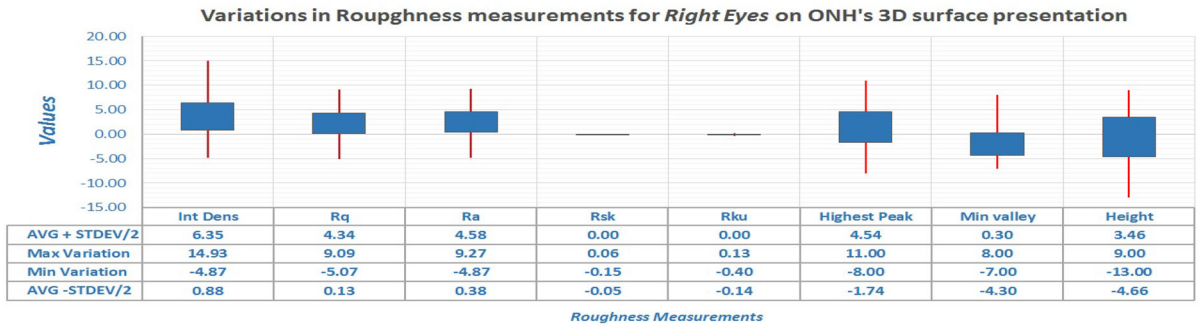


| | Int Dens | Rq | Ra | Rsk | Rku | Highest Peak | Min valley | Height |
|---|---|---|---|---|---|---|---|---|
| AVG + STDEV/2 | 6.35 | 4.34 | 4.58 | 0.00 | 0.00 | 4.54 | 0.30 | 3.46 |
| Max Variation | 14.93 | 9.09 | 9.27 | 0.06 | 0.13 | 11.00 | 8.00 | 9.00 |
| Min Variation | -4.87 | -5.07 | -4.87 | -0.15 | -0.40 | -8.00 | -7.00 | -13.00 |
| AVG -STDEV/2 | 0.88 | 0.13 | 0.38 | -0.05 | -0.14 | -1.74 | -4.30 | -4.66 |

**Fig. 6** A chart showing the MIN, MAX, and AVG ± STDEV values of the disparities in the eight roughness parameters on the right eyes 3D ONH surface during the follow-up attendances

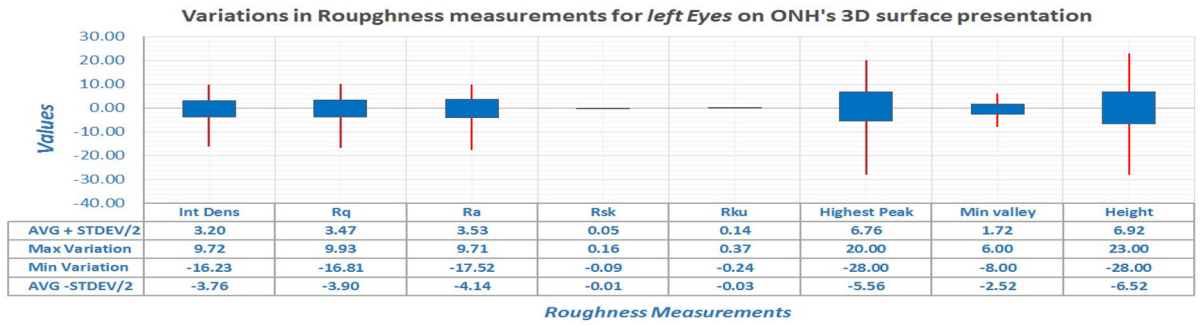


| | Int Dens | Rq | Ra | Rsk | Rku | Highest Peak | Min valley | Height |
|---|---|---|---|---|---|---|---|---|
| AVG + STDEV/2 | 3.20 | 3.47 | 3.53 | 0.05 | 0.14 | 6.76 | 1.72 | 6.92 |
| Max Variation | 9.72 | 9.93 | 9.71 | 0.16 | 0.37 | 20.00 | 6.00 | 23.00 |
| Min Variation | -16.23 | -16.81 | -17.52 | -0.09 | -0.24 | -28.00 | -8.00 | -28.00 |
| AVG -STDEV/2 | -3.76 | -3.90 | -4.14 | -0.01 | -0.03 | -5.56 | -2.52 | -6.52 |

**Fig. 7** A chart showing the MIN, MAX, and AVG ± STDEV values of the disparities in the eight roughness parameters on the left eyes 3D ONH surface during the follow-up attendances

suggested on single OCT ONH cross section [9], the 3D presentation of the ***entire*** ONH surface was generated and analyzed. This ONH surface appearance is not presented in SPECTRALIS, although it is possible as suggested in Fig. 2. The inclusive surface of the OCT ONH region is 3D visualized as seen in Fig. 4. This *would allow to visually look closer on disparities, if any, in OCT ONH shape during follow-up glaucoma patients*. This could complement the common OCT presentations that are used to diagnose patients' eyes. This is the first contribution in this paper. (We consider this as the main finding in this paper). The computer scientists can build up further displays. We suggest overlaying successive 3D ONH surfaces into single 3D display to observe or calculate differences, if occur. We did not do such to keep the number of figures and size of paper to the required limits.

On the other hand, the coronal slices of the OCT ONH were reconstructed as seen in the supplementary file (The coronal slices of OCT ONH region). This video showed the OCT ONH serial coronal slices, beginning at vitreous face till the bottom of the ONH valley (Lamina Cribrosa). Although it was straightforward generated from the OCT B-scan mode (Fig. 2), this video is also not presented in SPECTRALIS. The frames in the video were accumulated to present the average intensity of ONH coronal slices in Fig. 3 in order to later generate the 3D ONH surface. Therefore, we suggest that *the 3D ONH surface* (Fig. 4) *and the OCT coronal ONH slices (supplementary video) may benefit calculating the common ophthalmology quantities* (*e.g., the ONH axial length, cup-to-disc ratio, optic disc and optic disc rim area, cup volume* [7, 8, 10]). They might also help researchers in segmentation and/or auto-detection of eyes diseases affecting the ONH region [19, 20]. This is the second contribution in this paper.

Quantitatively, roughness parameters provided calculable proofs to observe ONH surface alterations during follow-up glaucoma patients. Figures 6 and 7 show that the roughness measurements $R_a$, $R_q$, $R_v$, $R_p$, and $R_t$, have higher disparity ranges than $R_{ku}$, and $R_{sk}$. Hence, the former parameters have the potential to observe the profiles of OCT ONH region surface. The $R_{IntDen}$ is not a roughness parameter; it is the integrated density of gray levels in an image (sum of pixels brightness). Figures 6 and 7 show that $R_{IntDen}$ is also possible to observe ONH variations. This allowed to conclude the third contribution of this paper. That is, *the roughness parameters and* $R_{IntDen}$ *are suggestive factors to monitor the disparities in the OCT ONH surface morphology that are due to eye diseases such as glaucoma*. There are other roughness parameters in ISO 25178-2 and ISO 4287-2000 [17, 18], which could also have been investigated. Investigation of all roughness parameters was beyond the objective of this paper.

From clinical point of view, Fig. 5 shows that, in case of glaucoma, there are inequalities of average roughness ($R_a$) for both right and left eyes. The figure shows that $R_a$ decreases or increases during the successive visits to ophthalmology clinic; the percentage of disparity was approximately in the range of 3–55% for both right and left eyes. We calculated the *percentage of disparity* in the ONH surface for other roughness parameters. Table 1 reports the MIN, MAX, AVG, and STDEV of the *percentage of disparity* for all roughness parameters. It shows that the percentage of variation can be as small as 3% or almost zero, but it can be as large as 56% or 100%. These variations are attributed to changes in the pressure of the intraocular pressure (IOP) in glaucoma patients during follow-up visits [4–7]. This leads to conclude that *the ONH surface presentation* (Fig. 4) *along with roughness measurements may complement other OCT presentations and parameters used in ophthalmology clinic to observe follow-up glaucoma patients*. This conclusion may be used for other eye diseases influencing ONH region such as optic disc swelling [3, 4]. This is the final contribution from experiments in this paper.

However, clinical factors need to be obtained in order to correlate between percentage disparities in 3D ONH surface waviness from one side (Table 1) and the progress of glaucoma on the other side. For examples, it would be needed to know the type and dose of medical prescription, severity of glaucoma, commitment to medicine schedule, and follow-up intervals for each glaucoma patient. Despite the necessity to know these clinical factors, it is clear from Figs. 4, 5, 6, 7 that there were variations in the shape of the ONH surface during the follow-up of the glaucoma patients due to alterations in the IOP. Therefore, the results suggest prospective clinical research toward investigating to which extent the disparities in 3D ONH surface associate with glaucoma. We propose to study the correlation of 3D ONH surface disparities (roughness measurements) with the well-established parameters used in glaucoma evaluation, e.g., RNFL, cup-to-disc ratio, or different volumes. This, however, would require large dataset to perform statistical analysis. This is out of the scope of this paper because it would increase the number of figures and tables as well as the text for discussion.

In the literature, the investigations of 3D visualization on OCT files have been explored since 2008 [12–16]. They all utilized *3*D volume rendering for volumetric visualization of the OCT macula [12, 13, 16], the OCT ONH geometry [12, 13], and/or the OCT laminar structure of ONH [14, 15]. Wang et al. (2016) used the 3D OCT volumetric data to calculate the ganglion cell complex, peripapillary thickness, RNFL, and ONH; they claimed that extracting quantities from the 3D OCT data should substantially improve diagnostic accuracy [12]. In

**Table 1** The MIN, MAX, AVG, and STDEV of the *percentage of disparity* (%) in the ONH surface during the follow-up visits

| | Percentage disparity in roughness parameters (%) | | | | | | | |
|---|---|---|---|---|---|---|---|---|
| | Int. dens. | $R_q$ | $R_a$ | $R_{sk}$ | $R_{ku}$ | Highest peak | Min valley | Total height |
| Right eye (OD) | | | | | | | | |
| MIN–MAX | 3–54 | 1–55 | 3–54 | 1–11 | 1–20 | 0–60 | 0–100 | 5–34 |
| AVG | 17 | 17 | 19 | 4 | 7 | 15 | 56 | 16 |
| STDEV | 17 | 18 | 18 | 4 | 7 | 16 | 43 | 8 |
| Left eye (OS) | | | | | | | | |
| MIN–MAX | 3–54 | 3–50 | 3–56 | 0–13 | 0–24 | 0 - 48 | 0–100 | 0–48 |
| AVG | 18 | 16 | 18 | 4 | 8 | 15 | 51 | 15 |
| STDEV | 16 | 15 | 16 | 4 | 9 | 17 | 40 | 17 |

contrast, in this paper, we attempted to display the surface of the ONH region (i.e., *3D surface rendering instead of 3D volume rendering*), as seen in Fig. 3 and 4. We developed different methods based on reconstruction of the OCT B-Scan mode (Fig. 2). This yielded to new presentation of ONH region called "the coronal slices of the OCT ONH region." Set of ISO roughness parameters (Figs. 5, 6, 7) were explored as new quantities that may possibly help in ophthalmology sciences. In summary, the methodology in this paper succeeded in presenting a new approximation to the entire ONH surface; this could help visual observation of the OCT ONH region's alterations during the follow-up visits; measurements of surface roughness were introduced.

Finally, it is important to explain an important technical point. That is the SPECTRALIS OCT device employed 24 out of 360 possible slices in the green circle (Fig. 1). If the 360 slices were utilized to generate the B-scan of the ONH (or higher number than 24 slices was used), there would have been no need for scaling in the third step. Consequently, this would have improved the approximation of the 3D ONH surface in Fig. 4, the fourth animation video (3D OCT ONH surface with rotation), and the measurements of roughness parameters in Figs. 5, 6, 7. Moreover, this would have allowed to present the ONH fundus photograph beside the ONH 3D surface morphology clarifying the ONH region for observation by ophthalmologist. We expect that if the SPECTRALIS OCT device allowed to obtain more than 24 OCT slices, this would have further demonstrated the worthiness (technical prospective) of the findings in this paper. Clinical evaluation is an upcoming research.

**Compliance with ethical standards**

**Conflict of interest** The authors declare that they have no conflict of interest.

**Ethical approval** The subjects in this experiment are *retrospective* OCT studies. The identifications of patients were removed from all patient's OCT files so they become anonymous OCT files.

## References

1. Frecher AF, Mengedoht K, Werner W (1988) Eye-length measurement by interferometry with partially coherent light. Opt Lett 13(3):186–188
2. Huang D, Swanson EA, Lin CP, Schuman JS, Stinson WG, Chang W, Hee MR, Flotte T, Gregory K, Puliafito CA, Fujimoto JG (1991) Opt Coherence Tomogr. Science 254(5035):1178–1181
3. Gelikonov VM, Gelikonov GV, Dolin LS, Kamensky VA, Sergeev AM, Shakhova NM, Galdkova ND, Zagaynova EV (2003) Optical coherence tomography: physical principles and applications. Laser Phys 13:692–702
4. Gabriele ML, Wollstein G, Ishikawa H, Kagemann L, Xu J, Folio LS, Schuman JS (2011) Optical coherence tomography: history, current status, and laboratory work. Investig Ophthalmol Vis Sci 52(5):2425–2436
5. Bussel II, Wollstein G, Schuman JS (2014) OCT for glaucoma diagnosis, screening, and detection of glaucoma progression. Br J Ophthalmol 98(Supplement):ii15–ii19
6. Töteberg-Harms M, Sturm V, Knecht PB, Funk J, Menke MN (2012) Repeatability of nerve fiber layer thickness measurements in patients with glaucoma and without glaucoma using spectral-domain and time-domain OCT. Graefes Arch Clin Exp Ophthalmol 250:279–287

7. Firat PG, Doganay S, Demirel EE, Colak C (2013) Comparison of ganglion cell and retinal nerve fiber layer thickness in primary open-angle glaucoma and normal tension glaucoma with spectral-domain OCT. Graefes Arch Clin Exp Ophthalmol 251:831–838
8. Savini G, Carbonelli M, Parisi V, Barboni P (2011) Repeatability of optic nerve head parameters measured by spectral-domain OCT in healthy eyes. Ophthalmic Surg Lasers Imaging 42:209–215
9. Al-Hinnawi AM, Al-Naami BO, Al-Latayfeh MM (2017) Optic nerve head slope-based quantitative parameters for identifying open-angle glaucoma on SPECTRALIS OCT images. Int Ophthalmol 37:979–988
10. Aref AA, Budenz DL (2010) Spectral Domain optical coherence tomography in the diagnosis and management of glaucoma. Ophthalmic Surg Lasers Imaging 41(Suppl.):S15–S27
11. Litjens G, Kooi T, Babak Bejnordi E, Setio AA, Ciompi F, Ghafoorian M, van der Laak JAWM, Ginneken B, Sánchez CI (2017) A survey on deep learning in medical image analysis. Med Image Anal 42:60–88
12. Wang B, Wollstein G, Schuman JS (2016) Optic nerve: optical coherence tomography. Pearls of Glaucoma Management. Springer, Berlin, pp 51–61
13. Ahdi A, Rabbani H, Vard A (2017) A hybrid method for 3D mosaicing of OCT images of macula and optic nerve head. Comput Biol Med. https://doi.org/10.1016/j.compbiomed.2017.10.031
14. Shoji T, Kuroda H, Suzuki M, Baba M, Araie M, Yoneya S (2015) Three-dimensional optic nerve head images using optical coherence tomography with a broad bandwidth, femtosecond, and mode-locked laser. Graefes Arch Clin Exp Ophthalmol 253:313–321
15. Kagemann L, Isikawa H, Wollstein G, Gabriele M, Schuman JS (2009) Visualization of 3D high speed ultrahigh resolution optical coherence tomographic data identifies structures visible in 2D frames. Opt Express 17(5):4208–4220
16. Zawadzki RJ, Fullerb AR, Choia SS, Wiley DF, Hamann B, Wernera JS (2008) Improved representation of retinal data acquired with volumetric Fd-OCT: co-registration, visualization and reconstruction of a large field of view. Proc SPIE. https://doi.org/10.1117/12.764070
17. ISO 4287:2000 Geometrical product specification (GPS)—Surface texture. Profile method. Terms, definitions and surface texture parameters
18. ISO 25178-2:2012 Geometrical product specifications (GPS) - Surface texture: areal - Part 2: terms, definitions and surface texture parameters
19. Yousefi S, Goldbaum MH, Balasubramanian M, Jung T, Weinreb RN, Medeiros FA, Zangwill LM, Liebmann JM, Girkin CA, Bowd C (2013) Glaucoma progression detection using structural retinal nerve fiber layer measurements and functional visual field points. IEEE Trans Biomed Eng 00:1–12
20. Koprowski R, Rzendkowski M, Wróbel Z (2014) Automatic method of analysis of OCT images in assessing the severity degree of glaucoma and the visual field loss. BioMed Eng (Online) https://doi.org/10.1186/1475-925x-13-16